Impact of Partial Linker Functionalization on the Catalytic Properties of MTV-UiO-66 for Biofuel Production

Asmaa Jrad [a], Mohamad Hmadeh [b,], Ghadir Awada [a], Ranim Chakleh [a] and Mohammad Ahmad [a,c,*]*

[a] Bahaa and Walid Bassatne Department of Chemical Engineering and Advanced Energy, Faculty of Engineering and Architecture, American University of Beirut P.O.Box, 11-0236, Beirut, Lebanon.

[b] Department of Chemistry, Faculty of Arts and Sciences, American University of Beirut P.O.Box, 11-0236, Beirut, Lebanon.

[c] Department of Chemical Science, University of Limerick, Limerick, V94 T9PX, Ireland

*Corresponding author: Mohamad Hmadeh

Email: mohamad.hmadeh@aub.edu.lb

*Corresponding author: Mohammad Ahmad

Email: ma258@aub.edu.lb

Keywords: MTV-MOFs, heterogeneous catalysis, structural defects, organic linker, regression modelling, biofuel additives.

Abstract

In this study, highly defected and functionalized metal-organic framework (MOF) structures are developed and exploited as catalysts for an esterification reaction for biofuel production. Two systems of multivariate UiO-66 series, namely MTV-UiO-66$(COOH)_2$ and MTV-UiO-66$(OH)_2$ incorporating dicarboxylate and dihydroxy groups, respectively, along with the single component structures, are thus explored for butyl butyrate production. Ratios of functionalized linkers to terephthalic acid are varied and a modulation synthesis approach is employed allowing for high levels of structural defects. The synthesized MOF structures are fully characterized using Powder X-ray diffraction (PXRD), thermogravimetric analysis (TGA), proton nuclear magnetic resonance (^{1}H-NMR), Brunauer−Emmett−Teller (BET), and scanning electron microscopy (SEM), and the results confirmed the homogeneous incorporation of the functionalized linkers in the structures. The combination of multivariate approach along with modulation synthesis yields structures with catalytic activity higher than those of highly defective fully functionalized structures and close to the homogeneous conventional catalyst used in esterification reactions. Moreover, the ratio of functionalized linkers to terephthalic acid is shown to be very important since not all MTV-UiO-66 performed better than the single-component structure which can be attributed to a combination of factors related to the density of active sites and their accessibility. The most active MTV-UiO-66$(OH)_2$ member, with 52% incorporation of functionalized linkers, a defects number of 1.9 out of 6, and a surface area of 761 m^2/g, yielded 92% conversion to butyl butyrate, compared to 95% for H_2SO_4, and its activity and stability is maintained over 4 consecutive cycles. Furthermore, by using the data of 33 different UiO-66 based catalysts for butyl butyrate production, a weighted linear regression model is suggested to predict the conversion based on the parameters that are concluded to mostly govern the catalytic activity of MOF catalysts. These parameters include the surface area, the catalytic loading, the defects number, and the level of incorporation of

BDC, and the functionalized linkers. The weights calculated for each of these parameters indicate that there is a more pronounced effect of active sites density on the conversion when compared to the surface area or the catalyst loading. These conclusions help pave the way for the engineering of MOF-based catalysts in the path of bridging the gap between homogeneous and heterogeneous catalysis for efficient biofuel production.

Graphical Abstract

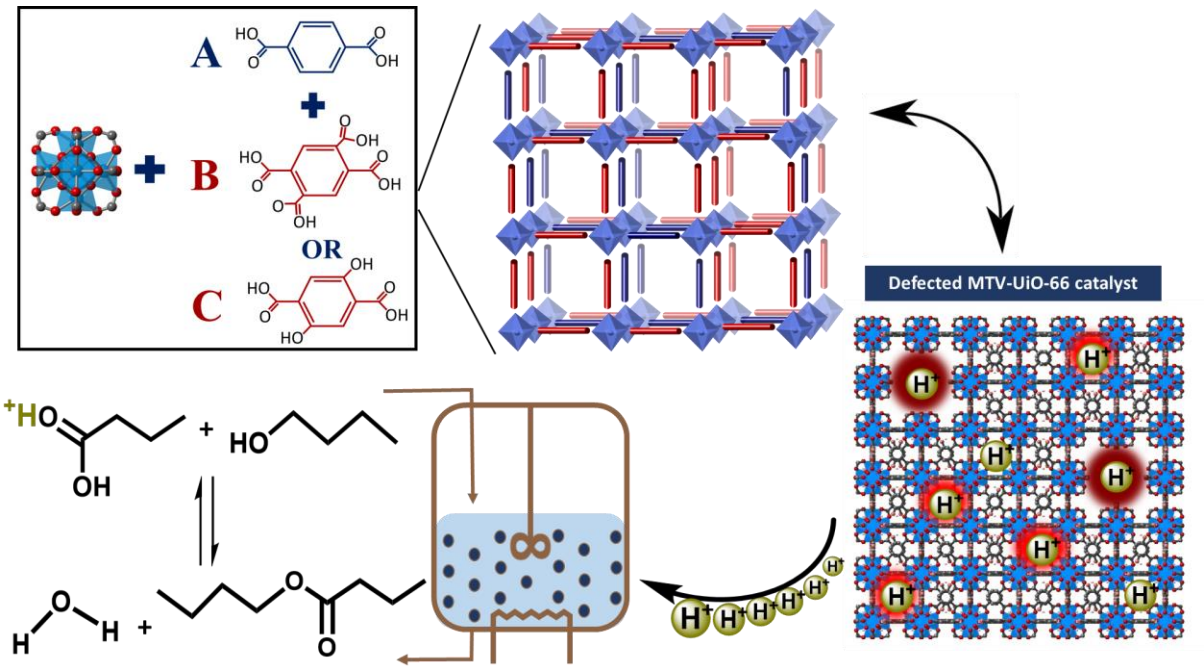

Two series of MTV-MOFs, MTV-UiO-66$(COOH)_2$ and MTV-UiO-66$(OH)_2$ are synthesized in a modulated synthesis approach yielding highly defected MTV-MOFs structures. Active sites are provided in the structure through the functionalized linkers, and the defected clusters. These active sites serve as the drive for the catalytic activity of the MTV-UiO-66 structures in the esterification reaction of butyric acid with butanol for butyl butyrate production.

Introduction

In order to lower the dependency on fossil fuels in the transportation sector and to limit the environmental and economic impact of energy consumption, biofuels and biofuel additives are gaining a lot of attention. [1-3] For instance, the fuel properties of butyl butyrate had been investigated and promising results were obtained when it had been blended with gasoline, biodiesel, and even aviation kerosene. [4, 5] Another interesting feature of butyl butyrate is that it is obtained from the esterification of butyric acid and butanol, and both reactants could be produced through biomass fermentation processes. [6] However, this esterification reaction is reversible and its yield in optimum reaction conditions is around 45% a without catalyst.[6] Therefore, this reaction is generally operated using convenient catalysts in the industrial sector, such as the conventionally used homogeneous acid catalysts. [7-9] These liquid acid catalysts, sulfuric acid, for example, yield a high conversion to butyl butyrate at a short period of time but cause many drawbacks like corrosion, product purification difficulty, recyclability issues, and many more. [10] These challenges have been the main reason behind the development of heterogeneous acid catalysts, which have their own limitations, especially regarding their catalytic activity, selectivity, design flexibility, diffusion limitations, and stability. [11-15] A real breakthrough in the catalysis field nowadays would be to develop a catalyst that could bridge this gap between homogeneous and heterogeneous acid catalysts to pave the way for efficient and environmentally friendly production of high-value chemicals like butyl butyrate. [16] This was the main reason behind the interest in the novel porous crystalline metal-organic frameworks (MOFs) in the catalysis field. [17] MOFs are hybrid materials assembled by bridging organic linkers and inorganic clusters into extended networks via strong bonds. On one end, MOFs offer a significantly high surface area, permanent porosities, a variety of active sites, and flexible design options. [18, 19] On the other end, MOF catalysts are heterogeneous, non-corrosive, easily separable from the reaction medium, and recyclable. [20] The previously

mentioned characteristics of MOFs have made them interesting in a wide variety of fields, especially that their functional groups could be tuned and altered for a specific application. [21-25] Some of the applications where MOFs are becoming famous include gas separation, [26] gas storage, [27, 28] water treatment, [29] chemical sensing, [30] and catalysis. [31]

Functional groups required in esterification reaction catalysts are mainly active acid sites, Brønsted or Lewis acid sites, as they allow for the activation of the carboxylic acid, which is then followed by the subsequent reaction with alcohol. Another reaction mechanism that can take place in an esterification reaction is the dual acid-base mechanism, where the basic sites form hydrogen-bonded adducts increasing the nucleophilic character of the alcohol's O atom, and favoring its reaction with the carboxylic acid. [32, 33] Active acid sites could be introduced into the MOF structure either through the organic ligand, the metal cluster, or the porous network. [34, 35] Additionally, Lewis acid sites could form on the cluster, because of defects, and could subsequently be altered into Brønsted acid sites through the adsorption of water molecules. [34, 35] These Lewis acid sites could be the result of the presence of structural defects caused by missing linkers or missing clusters in the MOF structure. [23, 35] The highly stable Zr-MOFs, for example, are particularly favorable in catalysis since defects could be systematically introduced into their structure, which increases their active sites density, surface area, and pore volume without affecting their stability. [23, 36, 37] On the other hand, Zr-MOFs could also be functionalized through their organic linker by incorporating additional active sites, acidic or basic, that are not coordinated to the cluster but rather participate in the adsorption and activation of reactants. [16, 23, 32, 38] The most famous and studied Zr-based MOF is UiO-66, which is known for its many functionalized iso-structures such as UiO-66(NH_2), UiO-66$(COOH)_2$, UiO-66$(OH)_2$ and many others. [32, 33, 39-41] Although the functional groups attached to the organic linkers add up to the active sites density in the structure, they have their drawbacks as well. Many studies have reported that the

functionalization of the UiO-66 structures is always accompanied by a significant decrease in the surface area of the structure and its pore volume. [32, 33, 41, 42] Most importantly, some studies raised the issue of internal diffusion limitations that seemed to be encountered in functionalized structures relative to the open non-functionalized UiO-66 framework. [32] As this was a concern that we had in our previous studies, [39, 40] we aimed at maximizing the catalytic activity of the synthesized structures by benefiting from the added active sites of functionalized linkers while maintaining high levels of surface areas and pores accessibility. This had shifted our attention to assessing the use of a multivariate MOFs approach, MTV-MOFs, which is based on mixing linkers incorporating different functionalities within the same topology. [43, 44] We were specifically interested in trying the isostructural mixed linkers approach, being relatively a simple way of introducing two or more organic linkers into the MOF structure. [45, 46] In the specific case of UiO-66, MTV-MOFs would incorporate two or more terephthalic acid derivatives as means to tune the properties of the structure especially in terms of surface area, porosity and reactivity. [47, 48] The change in the MTV-UiO-66 properties will depend on the ratio between the different linkers incorporated within the MOF crystals. This level of incorporation will have to be determined by ^{1}H-NMR spectroscopy. [49] While most reports focus on the importance of the cluster reactivity to boost the catalytic activity of the MOF catalysts, [18, 36, 50-54] less reports focus on the combination of the cluster activity with the linker functionalization. [40] Furthermore, and to the best of our knowledge, there haven't been any reports that focus on the optimization of the MOF catalytic activity for esterification reactions by combining the MTV-MOFs approach and the intentional introduction of defects into the cluster. To this end, the aim of this study is to maximize the catalytic activity of the UiO-66-based MOF structure, while mitigating the potential negative impact of the linkers' functionalization on the surface area levels and the accessibility of the internal active sites. This encouraged us to perform a study in which the linkers of UiO-66 are

partially functionalized in a controlled manner through the synthesis of MTV-MOFs. In addition to terephthalic acid, either 1, 2, 4, 5-benzenetetracarboxylic acid (MTV-UiO-66($COOH)_2$) or 2,5-Dihydroxyterephthalic acid (MTV-UiO-66($OH)_2$) are added to the reaction mixture. The modulation synthesis condition used for all synthesized structures is set to the optimal obtained in our previous study in order to ensure maximized defectiveness and, thus, activity on the Zr-cluster. [40] The ratio between the two linkers in each structure is varied to study its effect on the structural properties of the MOFs and their catalytic activity. After their synthesis, all MOF structures are fully characterized using powder X-ray diffraction (PXRD), N_2 sorption-desorption, thermogravimetric analysis (TGA), proton nuclear magnetic resonance (^{1}H-NMR), and scanning electron microscopy (SEM). The synthesized MOFs are then tested as catalysts for the esterification reaction of butyric acid in presence of butanol for butyl butyrate production. Furthermore, to highlight the MOF properties that govern the catalytic activity and primarily affect the conversion to butyl butyrate, a weighted linear regression model is developed to help put the results obtained into context. This study will thus provide basic knowledge and guidelines about the materials engineering tools required to maximize the potential of the emerging MOF catalysts for the purpose of biofuel additives production through esterification reactions.

1. Experimental section

Materials and general synthesis procedures

Chemical reagents used for MOFs synthesis, characterization, and testing in the esterification reaction were commercially purchased and used directly without further purification. The supporting information file comprises the details on the suppliers of products used in this study.

Nine different MOF catalysts incorporating single or mixed linkers were synthesized by a solvothermal modulated method using N,N-dimethylformamide as a solvent and formic acid

as modulator at 120 °C. The synthesis of the nine MOF samples is summarized in Scheme 1. The single linker MOFs synthesized are UiO-66, UiO-66$(COOH)_2$, and UiO-66$(OH)_2$. For the synthesis of UiO-66, 344 mg of $ZrCL_4$ (1.48 mmol) were dissolved in 40 mL of DMF (516.74 mmol) along with 245 mg of terephthalic acid (1.48 mmol). 11 mL of formic acid were then added to the mixture which was placed in a 100 mL vial, and the mixture was agitated in the sonicator for around 10 minutes. The homogenized mixture was then placed in a preheated oven at 120 °C for 21 hours. After 21 hours in the oven, the vials are removed, allowed to cool to room temperature, and the precipitated powder is collected from the synthesis solution by centrifugation. The obtained as-synthesized MOF is washed with DMF three consecutive times, allowing it to settle for at least 2 hours in between, and it is then similarly washed with DCM. After separating MOF from DCM following the last wash, MOFs are moved to a glass vial and is placed in a vacuum oven at 170 °C overnight for thermal activation. Full characterization of MOF then takes place.

The synthesis of UiO-66$(COOH)_2$ and UiO-66$(OH)_2$ occurred in the same manner by replacing the terephthalic acid in the synthesis mixture with 376 mg (1.48 mmol) of 1, 2, 4, 5-benzenetetracarboxylic acid and 293 mg (1.48 mmol) of 2,5-dihydroxyterephthalic acid respectively. Six MOFs were synthesized using MTV approach, with three catalysts incorporating both terephthalic acid and 1, 2, 4, 5-benzenetetracarboxylic acid, and the other three incorporating both terephthalic acid and 2,5-Dihydroxyterephthalic acid. The starting molar ratio of the two linkers was changed between 3:1, 1:1, and 1:3 with the total number of mole of both linkers being equivalent to 1 with respect to the number of moles of $ZrCl_4$ in the synthesis mixture. More details on the synthesis procedures of the MTV-MOFs can be found in the supporting information file in **Table S1**. **Scheme 1** is an illustration of the MOFs synthesis conditions and it displays the corresponding MOF nomenclature that will be adopted throughout the paper.

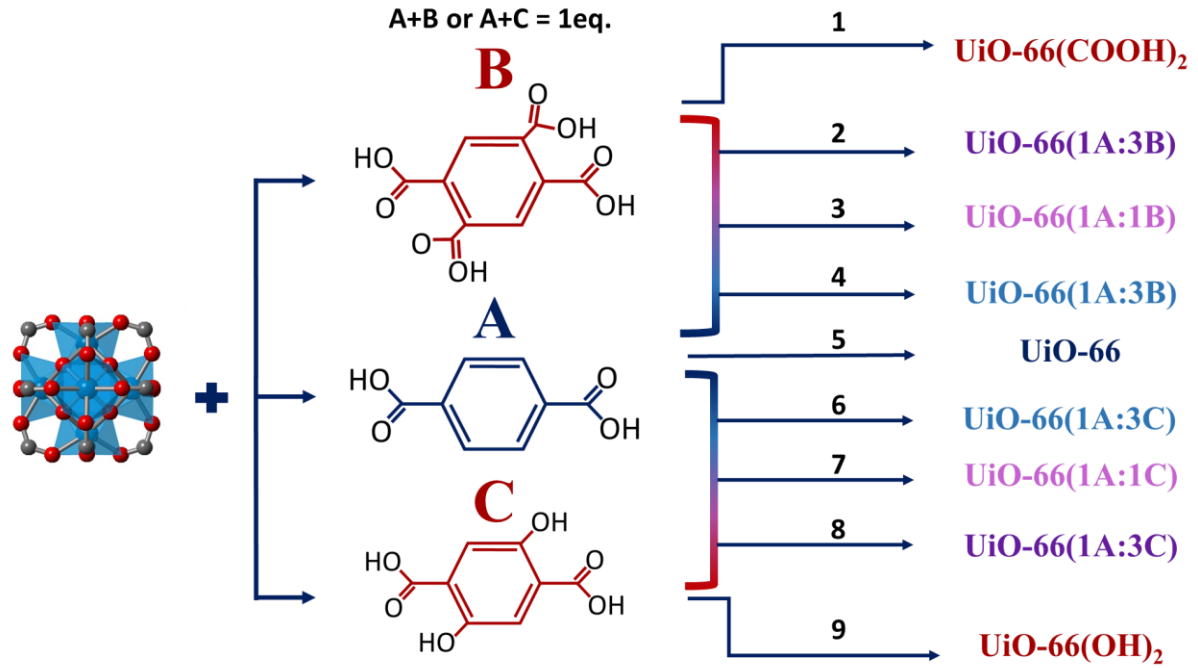

Scheme 1: Schematic illustration of the synthesis details of the 9 tested MOF catalysts. 1 eq. is one molar equivalent with respect to $ZrCl_4$ in the synthesis mixture

Catalyst characterization

After their synthesis, washing, and activation, the obtained MOF crystals are fully characterized. Powder X-ray diffraction patterns (PXRD) are recorded on a Bruker D8 advance X-ray diffractometer using Cu Kα radiation (k=1.5418 Å) working at 40 kV and 40 mA current, with the 2θ range being 2-50°, at an increment of 0.02° (Bruker AXS GmbH, Karlsruhe, Germany). Thermogravimetric analysis (TGA) of the synthesized MOFs is performed to assess their thermal stability and determine their defects number. 5-10 mg of the MOF sample are weighed using a microbalance and are placed in a platinum crucible for this purpose. The crucible is then placed in the auto-sampler of the Netzsch TG 209 F1 Libra TGA apparatus where the sample is placed inside the oven, heated in presence of air from 30 °C to 1100 °C, at a heating rate of 10 K. min^{-1}. Scanning electron microscopy (SEM) is used to assess particle size and crystal morphology. A very small quantity of each MOF sample is placed on an

aluminium SEM specimen stub that is covered with a conductive carbon tape, and the sample is then coated with around 25 nm layer of gold. The stub is placed in the MIRA3 Tescan electron microscope for SEM imaging. The samples' surface area and pore volume are assessed using N_2 sorption measurements at 77K in a Micrometrics Gemini VII 2390p surface area analyser. Before their analysis, samples are degassed overnight under a nitrogen flow at 170 °C. To evaluate the degree of incorporation of each of the linkers used in the MTV-MOFs, proton nuclear magnetic resonance (^{1}H-NMR) spectra are acquired on an AC500 Bruker spectrometer (^{1}H and ^{13}C NMR at 500 MHz). 5 mg of MOF samples are placed in ^{1}H-NMR tube and dissolved in a 1M $NaHCO_3$ solution in D_2O solvent under sonication for 30 minutes. Chemical shifts are recorded in delta (δ) units and expressed as ppm values relative to the internal standard Tetramethylsilane (TMS).

Esterification reaction

MOFs are tested as catalysts in the esterification reaction of butyric acid in presence of butanol for butyl butyrate production. In a 50-mL two-way round bottom flask, 5 mL of butyric acid and 10 mL of butanol are added [6]. The catalyst loading used in all of the reactions is 1 wt % with respect to the initial mass of butyric acid added, which is equivalent to around 50 mg of MOF. The reaction occurs under reflux in a round-bottom flask at a temperature of 110 °C and a constant stirring speed of 500 rpm using a magnetic stirrer/heater. The reaction is allowed to run for 24 hours and samples are regularly taken using an electronic micropipette. Samples are taken once every 2 hours for the first 8 hours, and then at 22 hrs, and finally at 24 hrs. The first sample is directly taken when the round bottom flask is placed in the oil bath and connected to the condenser. Collected samples are diluted in a 2 mL solution of heptane containing octanol at 10 mg/mL concentration, where octanol serves as an internal standard for Gas Chromatography (GC) analysis. Samples are then moved to a GC vial and placed in the GC auto-sampler for analysis. Thermo Scientific, Trace GC Ultra which is equipped with a Supelco

capillary wax column (30 m × 0.32 mm × 0.25 µm) is used for the GC analysis, and using the calibration curves for the reaction, the evolution of the concentration of each component in the reaction medium with time is determined. At the end of the reaction, MOF powder is extracted from the reaction medium using centrifugation and washed with DMF and DCM as detailed earlier in the synthesis section. The MOFs are then again activated in a vacuum oven at 170 °C and are characterized with PXRD to ensure samples remain stable after serving as catalysts in the esterification reaction. All reactions are repeated at least three times to confirm the reproducibility of the results.

2. Results and discussion

Structural Characterization

a) Powder X-ray diffraction (PXRD)

Before PXRD patterns recording, the MOF samples were placed in a vacuum oven at 120°C for 72 hours to ensure most of the solvent molecules trapped inside the pores are removed. This is important to dilute the effect of the solvation that is known to cause cell expansion while avoiding dehydroxylation of the structures which cause cell contraction. [47, 55] The recorded PXRD patterns of the 9 synthesized MOF samples are shown in **Figure 1** and reveal well-defined peaks that are in complete agreement with the simulated patterns for UiO-66, which indicates the high crystallinity and the phase purity of all the samples. In the case of a physical mixture with two phases present, it is expected that the peaks would be split or show shoulder peaks [55], which is obviously not the case as is clear in **Figure 1**. Moreover, **Figure S1** in the SI file displays a narrow 2theta range of the pattern that highlights a slight shift to a lower angle of the characteristic peaks of the MOF structure upon the increased incorporation of the functionalized linkers for both series of MTV-MOFs. This reflects a cell expansion caused by the gradual introduction of functionalized ligands in the structure which is reported previously for other MTV-MOFs, but highlighted herein for the first time for these structures. The

synthesized structures thus seem to follow Vegard's law confirming further the overall homogeneous incorporation of the functionalized linkers in the MOFs and that any potential short-range heterogeneity does not seem to have an important effect. [47, 55] Peaks that figure in the pattern recorded for UiO-66 are the narrowest, and those of UiO-66(COOH)$_2$ are the broadest. This reveals a smaller particle size of the functionalized structures as will be further discussed with SEM results.

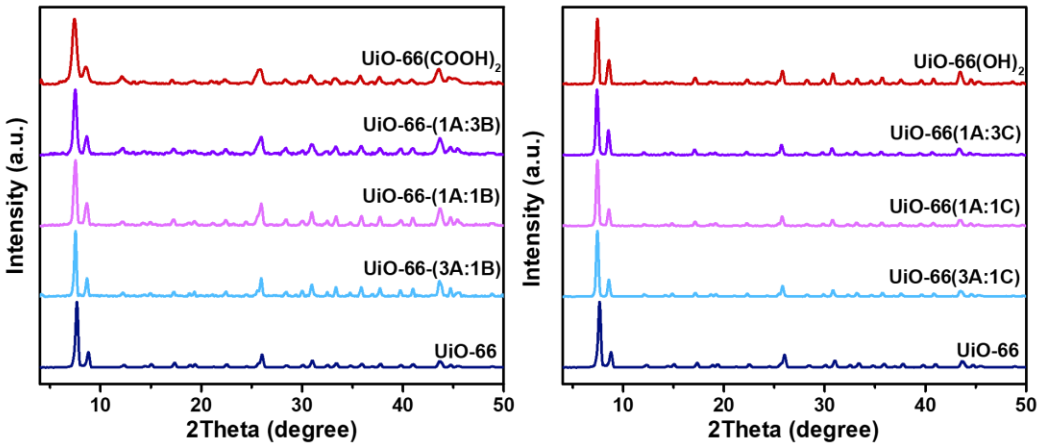

Figure 1: PXRD patterns of the activated single component and MTV-UiO-66 catalysts synthesized

b) Proton Nuclear Magnetic Resonance (^{1}H-NMR)

^{1}H-NMR spectra were recorded to monitor the level of incorporation of each linker in all synthesized samples and results are shown in **Figures S2** to **S7** in the supporting information file. A singlet at a chemical shift δ of around 8.43 ppm is present in all spectra and it was attributed to the residual DMF inside the pores of the MOFs. The aromatic zone of the ^{1}H-NMR spectrum reveals a singlet at around δ=7.85 ppm in all spectra as well and it is attributed to the four equivalent aromatic protons of the terephthalic acid. For MTV-MOFs, a singlet appears at δ=7.49 ppm in the spectra of the structures synthesized with the addition of 1,2,4,5-benzenetetracaboxylic acid, for which this singlet had been attributed. Similarly, a singlet is

present at δ=7.29 ppm for structures synthesized with the addition of 2,5-dihydroxyterephthalic acid for which this singlet was attributed. The percentage of actual incorporation of each of the linkers in every structure was calculated based on the results of the ^{1}H-NMR spectra obtained and the results are shown in **Figure 2**. As can be seen, the gradual increase in the amount of the functionalized linker in the synthesis mixture led to an increase in the percent ratio of their actual incorporation in the framework as reflected by the increasing intensity of the ^{1}H-NMR signals associated with these linkers (**Figure 2**). This clearly demonstrates the incorporation of both organic linkers in the MOF crystals. However, it seems that the level of incorporation was preferential with respect to terephthalic acid for both MTV-MOF systems as it is always higher than the starting molar ratios used.

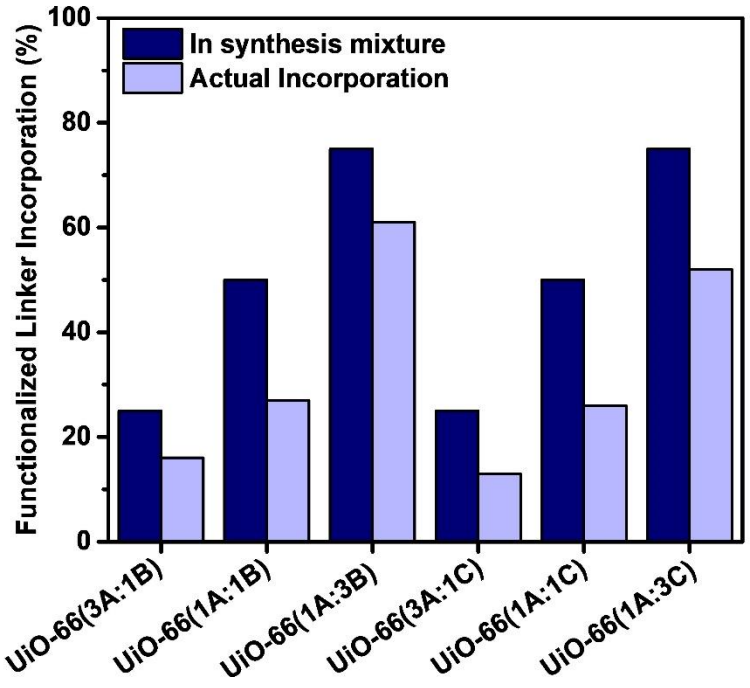

Figure 2: A comparison between the starting percentage of functionalized linker versus its actual incorporation in the framework of the different MTV-MOFs as determined from ^{1}H-NMR. The functionalized linker being 1,2,4,5-benzenetetracarboxylic acid in UiO-66(3A:1B), UiO-66(1A:1B) and UiO-66(1A:3B), and 2,5-dihyroxyterephthalic acid in UiO-66(3A:1C), UiO-66(1A:1C) and UiO-66(1A:3C).

c) Scanning Electron Microscopy (SEM)

Figure 3 shows the SEM images taken for all the 9 MOF structures synthesized. Particle sizes for all synthesized MOFs are also calculated based on PXRD patterns using the Scherrer equation and are reported in **Table 1**. UiO-66 crystals have a clear octahedral shape with the highest particle size among other samples (331 nm). MTV-MOFs constructed with the addition of the 1,2,4,5-benzenetetracarboxylic acid, namely UiO-66(3A:1B), UiO-66(1A:1B), and UiO-66(1A:3B), seem to have crystals with particle sizes decreasing with the decreased level of incorporation of terephthalic acid. Their particle sizes seem to decrease from levels similar to UiO-66 (331 nm) until they become similar to that of UiO-66$(COOH)_2$ crystals (28 nm) which reveal small inter-grown spheres. This trend is not maintained for the MTV-MOFs incorporating 2,5-dihyroxyterephthalic acid, namely UiO-66(3A:1C), UiO-66(1A:1C), and UiO-66(1A:3C), as they all seem to have similar small particle sizes around 50 nm with sphere-like morphology, while UiO-66$(OH)_2$ reveal bigger clear truncated octahedral crystals (252 nm).

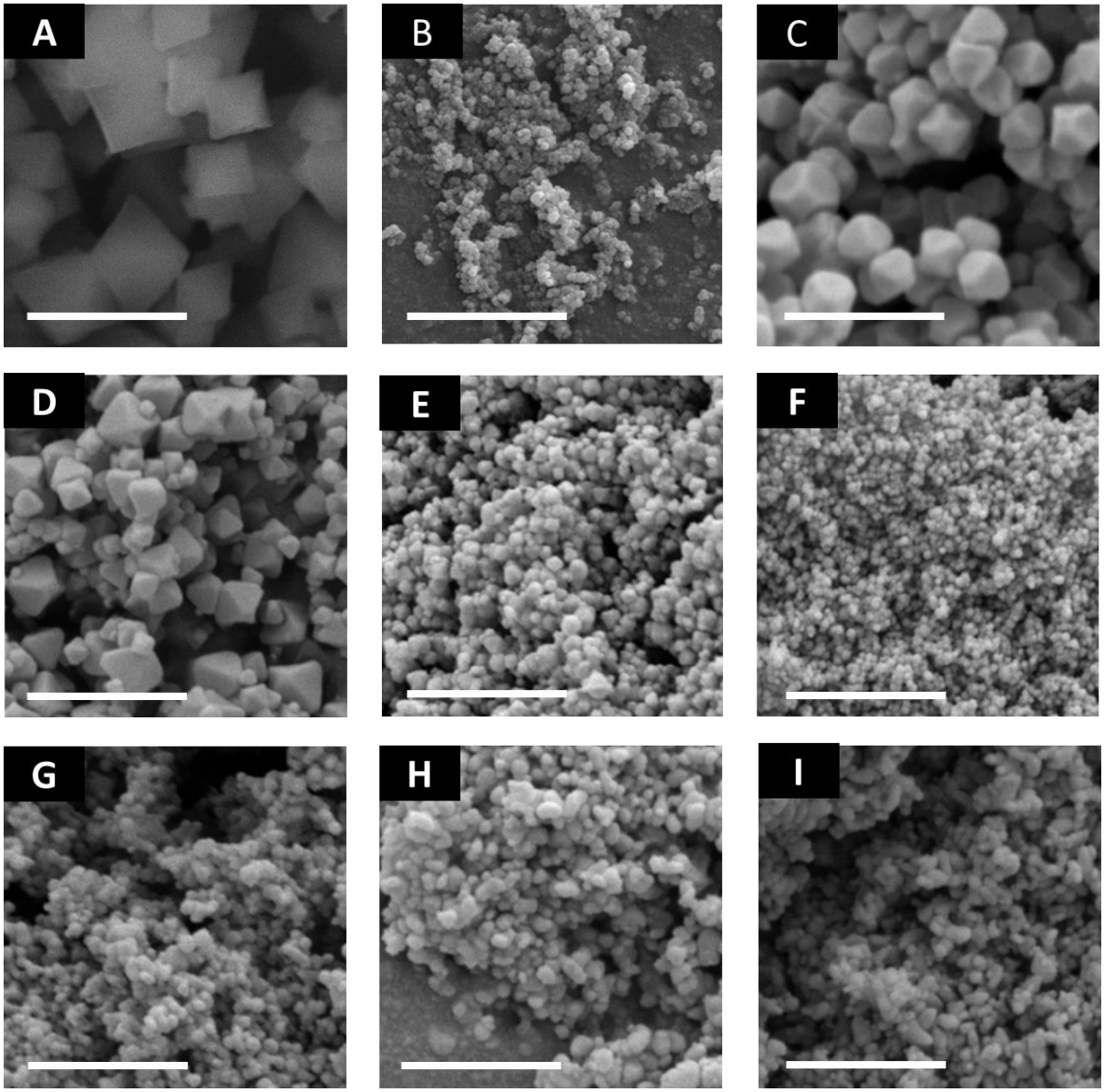

Figure 3: SEM images at a 1 μm scale bar for single component and MTV-UiO-66 catalysts synthesized. A: UiO-66 - B: UiO-66(COOH)$_2$ - C: UiO-66(OH)$_2$ - D: UiO-66(3A:1B) E: UiO-66(1A:1B) - F: UiO-66(1A:3B) - G: UiO-66(3A:1C) - H: UiO-66(1A:1C) - I: UiO-66(1A:3C).

d) Surface area analysis

Figure 4 shows the nitrogen sorption isotherms of all synthesized MOFs which are recorded at 77K. As expected, type I isotherms are obtained for all MOF crystals which is in accordance with the microporous nature of MOFs. As can be seen, the different levels of incorporation of the functionalized organic linkers within the MOF structures caused a significant change in their nitrogen uptake. For all structures tested, the increase in the level of incorporation of

functionalized linkers in the structure had caused a subsequent decrease in the nitrogen uptake. Additionally, MTV-UiO-66(OH)$_2$ comprising terephthalic acid and 2,5-dihydroxyterephthalic acid, UiO-66(3A:1C), UiO-66(1A:1C), and UiO-66(1A:3C), had higher levels of surface areas than MTV-UiO-66(COOH)$_2$ having terephthalic acid and 1,2,4,5-benzenetetracarboxylic acid, UiO-66(3A:1B), UiO-66(1A:1B), and UiO-66(1A:3B). This could be because the carboxylic functional groups are bulkier than the hydroxyl groups. In general, the increased incorporation of functionalized linkers seemed to decrease the accessibility of the porous network of MOF samples which is reported previously for other MTV-MOF systems. [56]

Table 1 reports the calculated Brunauer–Emmett–Teller (BET) surface areas and the pore volumes of the activated MOF samples. In accordance with the nitrogen uptake observations, the level the of surface area is noticeably decreasing with the increased levels of functionalized BDC inside the framework. This decrease in surface area is more significant in MTV-MOF-(COOH)$_2$ where the surface area drops from 1290 m^2/g for UiO-66(1A:3C) to 760 m^2/g for UiO-66(3A:1C). Moreover, the calculated pore volumes follow the same trend. **Figure 4** shows the change in the surface areas of synthesized MOFs with respect to the level of incorporation of functionalized linkers within the framework. It could be seen that the decrease in surface area is significant upon the introduction of an even low percentage of functionalized linkers to the structure.

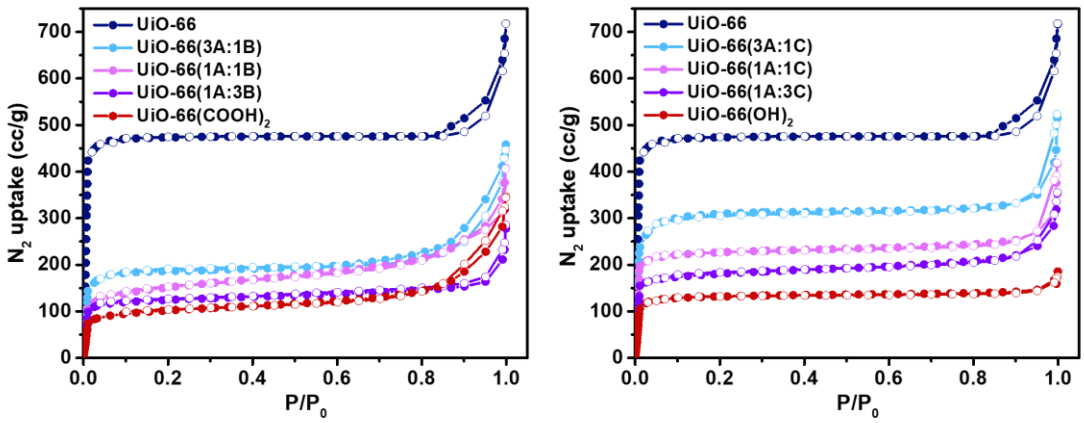

Figure 4: Nitrogen adsorption-desorption isotherms for all synthesized MOF catalysts synthesized. • Adsorption ◦ Desorption.

Table 1: Quantitative results extracted from the characterization and testing of all the MOF catalysts.

MOF	BET surface area (m^2/g)	Pore volume (cm^3/g)	Defects number	Particle size (nm)	Conversion to butyl butyrate
UiO-66	1812	0.73	1.87	331	75.1
UiO-66(COOH)$_2$	522	0.11	1.93	28	76.6
UiO-66(OH)$_2$	602	0.19	1.51	252	80.5
UiO-66(3A:1B)	773	0.26	1.83	302	70.3
UiO-66(1A:1B)	657	0.16	2.14	83	85.3
UiO-66(1A:3B)	609	0.16	1.98	38	88.8
UiO-66(3A:1C)	1290	0.46	1.33	45	72.5
UiO-66(1A:1C)	947	0.33	1.73	55	86.5
UiO-66(1A:3C)	761	0.24	1.90	51	92.2

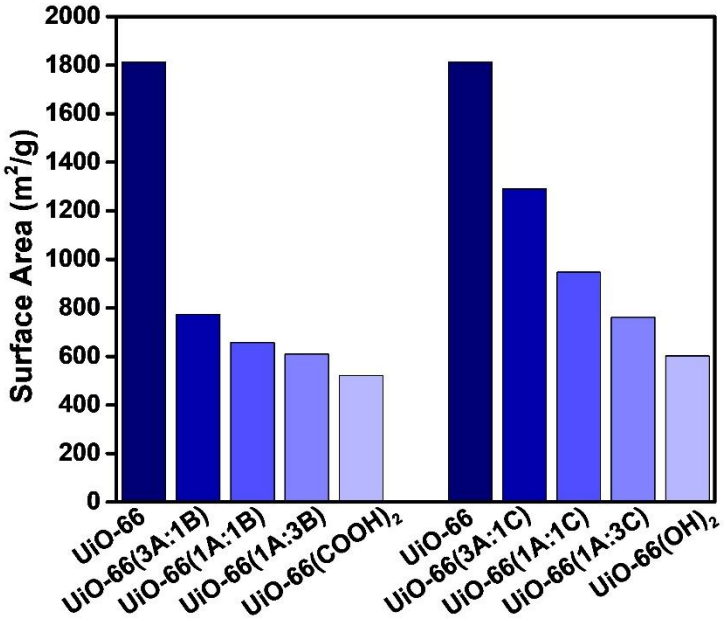

Figure 5: Decreasing levels of BET surface area with the increased percentage of incorporation of the functionalized organic linkers in the MOF structure

e) Thermogravimetric Analysis (TGA)

The Thermal stability and structural defects of the synthesized samples were assessed using TGA which shows the change of the mass percentage of the samples while increasing the temperature between 30 °C and 1100 °C, and the results are shown in **Figure 6**. Following a well-established method in the literature for defects number calculation, [50] the TGA curves were normalized so that the final weight loss is 100% as illustrated in **Figure 6**. As can be seen in the figure, the thermal stability of the pure UiO-66 was higher than that of both pure functionalized structures, namely UiO-66$(COOH)_2$ and UiO-66$(OH)_2$. The decreased stability of the functionalized structures was attributed in previous studies to the lower metal-linker interaction in the functionalized structures when compared to pure UiO-66. [47] The thermal stability of MTV-MOF structures had fluctuated in between those of both single component structures as could be seen in the TGA curves in **Figure 6**. The shift in thermal stability in MTV-MOFs is more pronounced in the MTV-MOF$(OH)_2$ systems, (UiO-66(3A:1C), UiO-

66(1A:1C), and UiO-66(1A:3C)), given the wider gap between the thermal stability of UiO-66 and UiO-66$(OH)_2$.

The number of defects for the single component structures is calculated following a method previously reported in the literature [50], which was also used for the MTV-MOF systems with minor changes in the calculation of the molecular weight of the cluster-linker unit. The molecular weight is calculated based on the level of introduction of each organic linker in the structure making it an average for the whole relevant structure. The defects number for UiO-66(3A:1B), UiO-66(1A:1B), and UiO-66(1A:3B) is estimated to be around 1.83, 2.14, and 1.98 out of 6 linkers per cluster respectively. An ascending defects trend with increased incorporation of the functionalized structure was noted for the second MTV-MOF system with 1.33, 1.73, and 1.90 missing linkers for UiO-66(3A:1C), UiO-66(1A:1C), and UiO-66(1A:3C) respectively. However, the number of defects for MTV-MOF structures are not bounded by that of single linker structures. Moreover, the number of missing linkers for UiO-66, UiO-66$(COOH)_2$, and UiO-66$(OH)_2$ is estimated to be around 1.87, 1.93, and 1.51 respectively. Having no direct correlation between the change in the number of defects and the decrease in the thermal stability of the MTV-MOF structures reflects the minimal effect of defects on the thermal stability of these structures. This further highlights that the decrease in the thermal stability was caused by the increased incorporation of the functionalized linkers that have weaker interaction with the cluster, which is previously reported for similar structures, but for the first time in this study for the studied systems [47, 55].

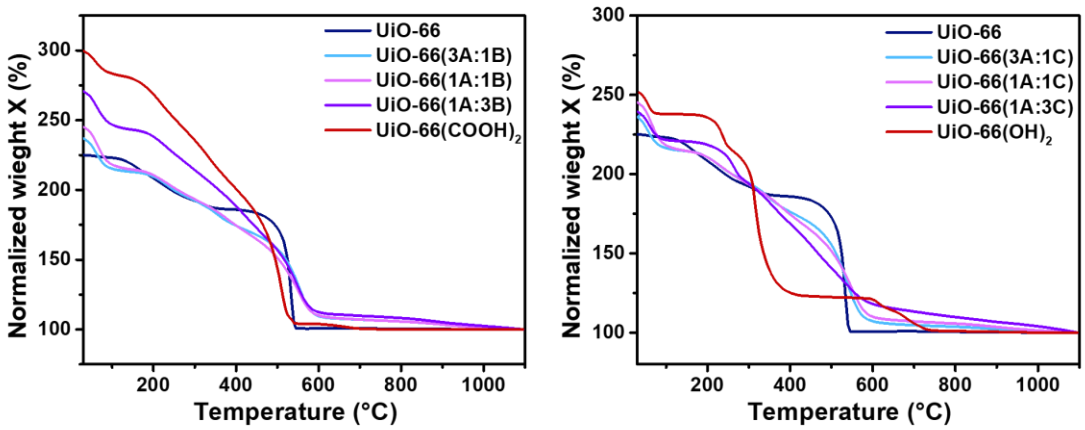

Figure 6: TGA curves of all synthesized MOF catalysts.

MOFs testing in esterification reaction for butyl butyrate production

a) Effect of the level of incorporation of the functionalized linkers

Activated MOFs are used as catalysts in the esterification reaction of butyric acid and butanol for butyl butyrate production. The reaction time was set to be 24 hours and only 1 wt% catalyst is used in this study, which is equivalent to around 50 mg of MOF powder. As a reference for MOFs catalytic activity, one reaction is allowed to occur without the use of a catalyst, noted Blank, and another reaction is performed under 1 wt% H_2SO_4. Samples were regularly taken from the reaction medium once every two hours for the first 8 hours, and at 22 hours and 24 hours, then these samples were analysed using GC.

The results of the evolution of the conversion to butyl butyrate with respect to time are shown in **Figure 7**, while **Figure 8** compares the conversion obtained using each MOF catalyst after 24 hours of reaction. No reactants other than butyl butyrate were detected in GC analysis which means that the selectivity to the desired product is 100%. Observing the performance of MOF catalysts with respect to time as illustrated in **Figure 7**, an interesting trend could be noted.

Starting with the MTV-MOF series, it is noticeable that for both systems, structures with 50% and 75% functionalized linker starting molar ratio had the highest catalytic activity. In fact, the increased conversion to butyl butyrate when using these MTV-MOF systems is more pronounced at the beginning of the reaction. Moreover, compared to UiO-66 which yields around 53% conversion to butyl butyrate after 8 hours of reaction, around 72% and 74% are obtained when using UiO-66(1A:3B) and UiO-66(1A:3C) respectively. In fact, the best performance is obtained when UiO-66(1A:3B) and UiO-66(1A:3C) catalysts are employed. To put these results into context, the structural characterization results obtained and reported in **Table 1** are discussed. Comparing UiO-66 and UiO-66(1A:3B), the first thing to notice is the higher active sites density of the latter given the higher defects number and the 61% level of incorporation of 1,2,4,5-benzenetetracarboxylic acid linkers with its COOH groups. Additionally, the particle size of UiO-66(1A:3B) is considerably smaller which increases the external surface area and thus the accessibility of active sites. This explains the higher performance of UiO-66(1A:3B) when compared to the open structure of pure UiO-66. On the other hand, when compared to UiO-66$(COOH)_2$, UiO-66(1A:3B) is characterized by much higher level of defectiveness and higher surface area, which could explain its better performance. Almost the same goes for the comparison between UiO-66 and UiO-66(1A:3C) where the latter, although having lower surface area, benefits a from higher level of active sites density, given the incorporation of 2,5-dihydroxyterephthalic acid up to 52% along with higher level of defects. However, in the case of MTV-UiO-66$(OH)_2$, the role of the active sites on the organic linker differs from that of the active sites on the cluster. While the cluster provides active acid sites, the OH groups are possibly favouring a dual acid-base activation mechanism as previously suggested by Cirujano et al. [32, 33] In such a mechanism, the butyric acid would adsorb onto the acid sites of the cluster, which increases the electrophilic character of the carbon atom in the carboxylic group. At the same time, the OH groups of the linker is thought

to form hydrogen-bonded adducts that increase the nucleophilicity of the O atom of the butanol's hydroxyl group, which could favour its reaction with the butyric acid (**Figure S8**). This reaction mechanism could explain the superior activity of this catalyst over its counterparts that are only acid catalysed. Observing other characteristics that might have contributed to the superior performance of UiO-66(1A:3C), it can be noted that it also benefits from smaller particle size relative to UiO-66, and has a higher surface area and defects number compared to UiO-66$(OH)_2$. This thus shows that the mixed-linker approach has a positive effect on increasing the level of active sites compared to the pure UiO-66 structure while maintaining higher surface area values when compared to the pure functionalized structures.

However, this trend could not be generalized, since not all MTV-MOF systems have better catalytic activity than their single-component counterparts. In fact, UiO-66 and UiO-66$(COOH)_2$ both performed better than UiO-66(3A:1B), while UiO-66 and UiO-66$(OH)_2$ both performed better than UiO-66(3A:1C). Although these MTV-MOFs have higher surface areas than their pure functionalized counterparts, namely UiO-66$(COOH)_2$ and UiO-66$(OH)_2$, and despite them having part of their linkers functionalized, these MTV-MOFs still had lower catalytic activity. When comparing the structural characteristics of UiO-66(3A:1B) with those of UiO-66, it could be noticed that the two structures have comparable defects number while UiO-66(3A:1B) has a much lower surface area. Additionally, relative to UiO-66$(COOH)_2$, UiO-66(3A:1B) has lower active sites density given both the lower defects number and the lower partial incorporation (16%) of functionalized linkers in the structure. Again, and as for UiO-66(3A:1C), its lower catalytic activity could be attributed to the noticeably lower defects number when compared to that of UiO-66 and UiO-66$(OH)_2$.

The best performing MOF, UiO-66(1A:3C), yields 92% conversion to butyl butyrate which is comparable to that obtained using 2 wt% of the best performing UiO-66$(COOH)_2$ structure in our previous study [40]. So in this study, we managed to synthesize materials of significantly

higher catalytic activity which yielded similar conversion to butyl butyrate compared to their counterparts even when half the catalytic loading is used. This reveals the successful implementation of the MTV-MOF strategy by benefiting from the advantages of both the open structure of UiO-66, the high active density of functionalized structures of UiO-66$(COOH)_2$ and UiO-66$(OH)_2$, along with the high number of defects from the addition of high concentrations of the formic acid modulator. Although H_2SO_4 still performed better than MOF catalysts, the gap between the performances of the two systems was lowered when using MTV-MOFs approach. Additionally, the final yield after 24 hours of the reaction using H_2SO_4 and the best performing MOF, UiO-66(1A:3C), was comparable being 95% and 92% respectively.

To ensure that the synthesized systems retain their activity, UiO-66(1A:3C) was washed following the reaction and recycled for four consecutive cycles, and the results are shown in **Figure S9** in the SI file. As could be seen, there is no noticeable change in the conversion to butyl butyrate over the cycles, which proves that the structure's activity is maintained. In addition, PXRD patterns of the recycled MOF were recorded to test the stability of the framework following four reaction cycles, and the results are shown in **Figure S10** in the SI. The PXRD pattern of the recycled structure is identical to that of the freshly synthesized MOF, which shows that the synthesized structures remain stable after recycling.

b) Effect of the organic linker steric bulk

After comparing the structures in terms of the level of incorporation of the functionalized linker, it is necessary to compare their performance with respect to the type of this linker being incorporated and the functional group it is adding to the structure (**Figure 9**). To begin with, the single component functionalized MOFs, which have lower surface area than pure UiO-66, both have relatively higher catalytic activity, which could be the result of the dangling functional groups on their linkers. This trend had been previously reported for UiO-66$(COOH)_2$ with relatively comparable defects number with UiO-66 [40], but this is reported for the first

time using UiO-66(OH)$_2$ which has considerably lower defects number than both pure counterparts. In fact, UiO-66(OH)$_2$ had 1.51 missing linkers per cluster compared to 1.86 and 1.93 missing linkers in the case of UiO-66 and UiO-66(COOH)$_2$ respectively, which is a gap in defectiveness that could potentially hinder the catalytic activity of a UiO-66-based MOF structure. However, while UiO-66 depends only on the number of defects to obtain open catalytic centres for the esterification reactions [36, 37], this is not the case for UiO-66(COOH)$_2$ and UiO-66(OH)$_2$. On the other hand, despite having no other active site than the defects, the catalytic performance of UiO-66 was comparable to its pure functionalized isostructures. The reason behind this is probably due to its open structure which allows for easier diffusion of the reactants inside the porous network and the subsequent access of the internal active sites [32, 57]. A similar approach could be used when analysing the results obtained using UiO-66(COOH)$_2$ and UiO-66(OH)$_2$. Although both MOFs contributed to similar conversion to butyl butyrate, UiO-66(OH)$_2$ has considerably lower defects number but slightly better conversion. Many parameters could have contributed to this result but the most obvious could be the functional group attached to the linker which differs in both systems. First, and as previously discussed, the different functional groups on the organic linkers of both systems is thought to cause different reaction mechanisms. While MOFs with COOH groups benefit from higher levels of acid active sites, the structures with OH groups benefit from a dual acid-base mechanism which is reported to increase the catalytic activity, as previously reported for systems with NH_2 groups, namely UiO-66(NH_2) [32, 33]. Additionally, the COOH groups seem to have a more pronounced negative effect on the diffusion of the reactants when compared to the less bulky OH groups. In fact, at this level of defects obtained in UiO-66(COOH)$_2$, its catalytic activity is expected to be higher, but diffusion problems could have made its catalytic centres less accessible [32, 57]. Additionally, the surface area is a critical parameter in heterogeneous catalysis as the activation and subsequent reaction takes place on

the outer surface of the catalyst. It is thus expected that having a catalyst with the same properties but with a higher surface area would have better catalytic activity. **Table 1** shows that UiO-66$(OH)_2$ has a higher surface area than that of UiO-66$(COOH)_2$ which could explain why UiO-66$(OH)_2$ performed better regardless of its lower defects density. This discussion could be extended to the MTV-UiO-66$(OH)_2$ systems which perform better than their single component UiO-66 counterparts despite their considerably lower defects density. Comparing UiO-66(3A:1B) to UiO-66(3A:1C), UiO-66(1A:1B) to UiO-66(1A:1C), and UiO-66(1A:3B) to UiO-66(1A:3C), these structures had a comparable level of incorporation of functionalized linkers in their structure and thus a comparable level of active sites density provided by the linker. However, the MTV-UiO-66$(OH)_2$ structures have a lower number of defects but consistently better catalytic performance. This could again attributed to the dual acid-base mechanism, and the lower steric bulk of the OH groups which allowed for better accessibility of the active sites. Additionally, MTV-UiO-66$(OH)_2$ structures have higher levels of surface area, which could be attributed to the higher surface area of UiO-66$(OH)_2$ when compared to its functionalized counterpart UiO-66$(COOH)_2$. This higher level of surface area would extend the surface for catalysis and reactants activation especially when the particle size of MTV-UiO-66$(OH)_2$ and MTV-UiO-66$(COOH)_2$ become comparable.

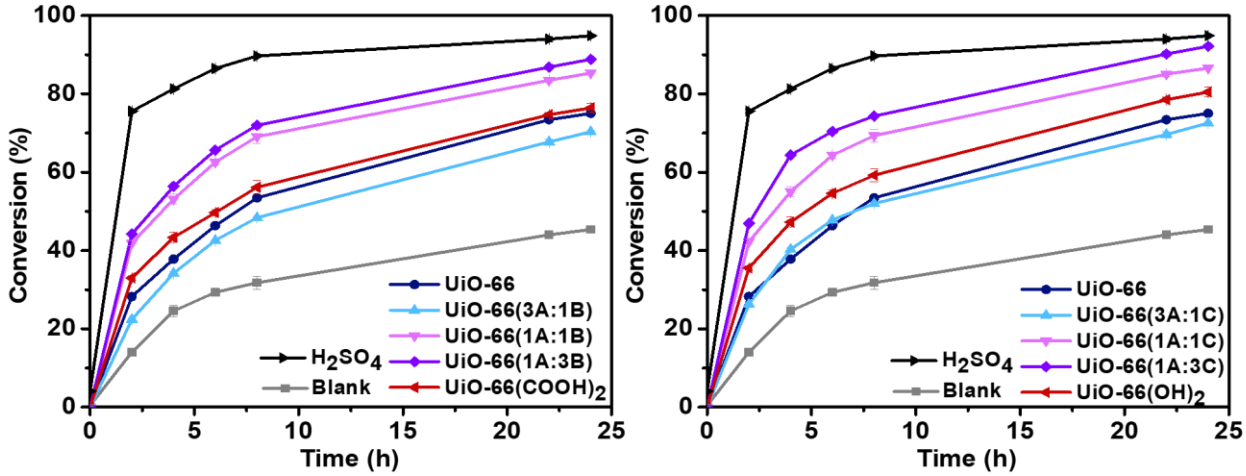

Figure 7: The conversion to butyl butyrate with respect to time using 1 wt% of each MOF catalyst

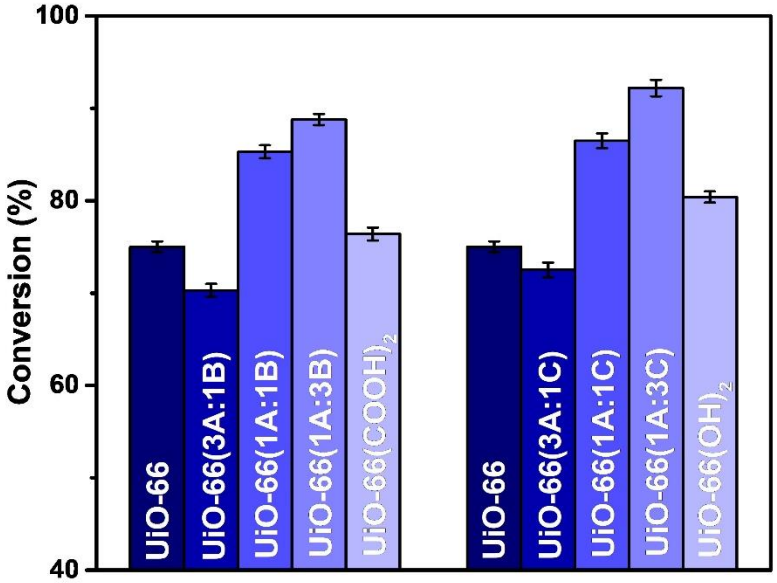

Figure 8: Final conversion to butyl butyrate after 24 hours of reaction under 1 wt% of each MOF catalyst

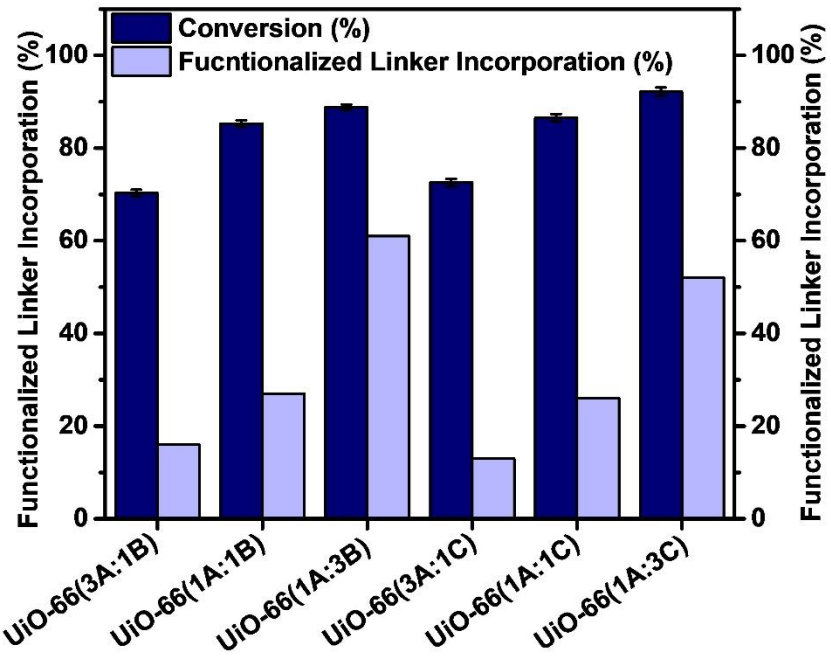

Figure 9: Change in conversion compared to change of the functionalized linker incorporation in MTV-MOFs structure

c) Regression Model

Following our previous studies on functionalized and defected UiO-66-based catalysts for the production of butyl butyrate, [39, 40] along with the present study, a simplified regression model is suggested to predict the final conversions. Moreover, our studies have focused in-depth on the effect of the different characteristics of MOFs on their catalytic activity, and it had been concluded that a few main characteristics mostly govern the conversion and appear to be critical in the engineering of new UiO-66 based catalysts for esterification reactions. Modeling was thus suggested to be used as it helps to (i) extract an empirical relationship between the MOFs characteristics and the conversion to butyl butyrate, (ii) provide a tool for conversion prediction without having to run the esterification reaction, and (iii) screen the characteristics used as input of the model to identify which ones are more important than others in increasing the yield of butyl butyrate [58]. This highlights the parameters that are more critical to engineer in a MOF structure in order to maximize its catalytic activity.

For this reason, a regression model is proposed to predict the catalytic activity of UiO-66-based MOFs taking into account these main characteristics as a general scheme to design and develop a MOF catalyst of better performance. To simplify the interpretation of model predicted conversion and to minimize the computational requirements of the model, a simple multiple weighted linear regression model is adopted to fit the data of the three studies. The output of the model would be the conversion to butyl butyrate and the parameters that were concluded to be governing the catalytic activity of the UiO-66-based catalysts were used as input. These mainly include the surface area, the number of defects, the catalyst loading, and the level of incorporation of the functionalized organic ligands in the MOF structure. These parameters had been changed throughout 33 different reactions performed in our studies and their actual values are depicted in **Table S2** in the supporting information file. **Table S3** represents the normalized values of the relevant parameters between 0 and 1. The normalization of the parameters allows for constructive discussion on the relative effect of each of them on the conversion to butyl butyrate. The suggested linear regression model is presented below:

$$Conv_{mod,i} = a * \%A_i + b * \%B_i + c * \%C_i + d * SA_i + f * CL_i + e * DN_i + Cst$$

Where:

i: is the number of experiments performed in our three studies which is 33

$Conv_{mod,i}$: is the model-predicted conversion to butyl butyrate based on the governing parameters of the MOF structure for experiment i

$\%A_i$: is the level of incorporation of the terephthalic acid linker in the MOF structure used in experiment i, which varies between 0 and 100% and is normalized between 0 and 1

$\%B_i$: is the level of incorporation of the 1, 2, 4, 5-benzenetetracarboxylic acid linker in the MOF structure used in experiment i, which varies between 0 and 100% and is normalized between 0 and 1.

$\%C_i$: is the level of incorporation of the 2,5-Dihydroxyterephthalic acid linker in the MOF structure used in experiment i, which varies between 0 and 100% and is normalized between 0 and 1.

SA_i: is the level of the surface area of the MOF used in experiment i, which varies between a minimum of 51 m^2/g and a maximum of 1813 m^2/g throughout the studies and is normalized between 0 and 1.

CL_i: is the catalyst loading used in experiment i, which varies between 1, 2, and 5 wt% throughout the studies and is normalized between 0 and 1.

DN_i: is the defects number of the MOF used in experiment i, which varies between 0.88 and 2.14 missing linkers out of 6 throughout the studies and is normalized between 0 and 1.

Cst: is the y-intercept of the model, when all parameters are equal to zero, or in other words, when no catalyst is being used.

$a, b, c, d, e, and\ f$: are the regression coefficients, or weights, attributed to each of the parameters chosen and are calculated using Microsoft Excel Regression Analysis, provided in the data analysis tool.

After setting the experimental conversion as the output to be predicted and the normalized values of the chosen parameters, as indicated in **Table S3,** as the independent variables to be used for the prediction, Excel Data Analysis was used to determine the suitable regression model as follows:

$$Conv_{mod,i} = 6.87 * \%A_i + 21.93 * \%B_i + 25.25 * \%C_i + 16.19 * SA_i + 15.38 * CL_i + 25.07 * DN_i + 39.94$$

Figure 10 depicts the correlation between the model-predicted conversion and the experimentally obtained conversion to butyl butyrate.

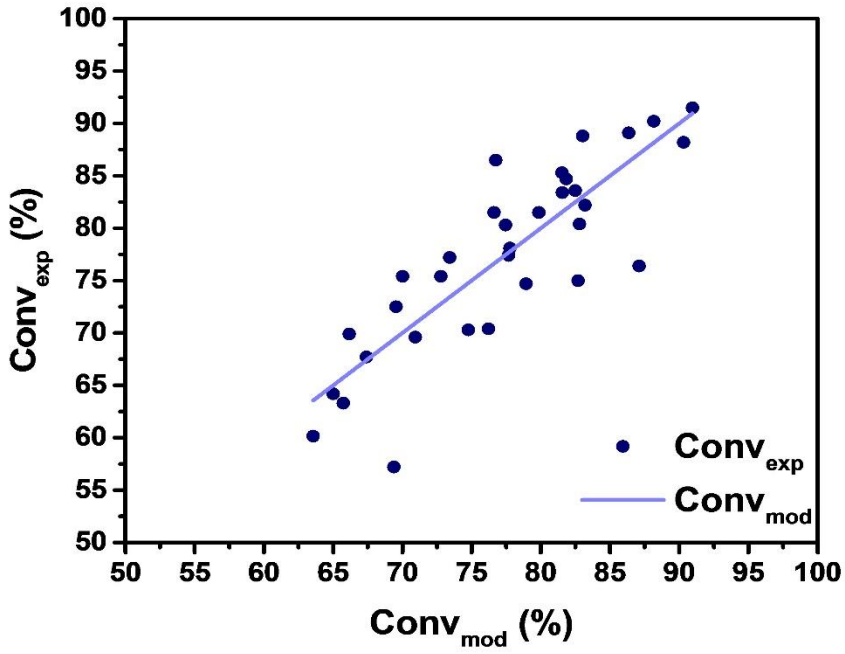

Figure 10: The correlation between the experimentally obtained conversion to butyl butyrate and the suggested linear model

Table S4 shows the calculated weights and intercept along with their P-Values which is an expression of the statistical significance. P-values that are less than 0.05 indicate strong evidence against the null hypothesis, which is the hypothesis that there is no relationship between the independent variable and the output to be predicted. Since the P-values of the chosen independent variables are all below 0.05 (**Table S4**), this reflects their suitability for the prediction of the conversion to butyl butyrate [58]. This reveals that our assumption of the relationship between the chosen MOFs characteristics and the conversion to butyl butyrate is statistically valid. The correlation coefficient Multiple R is shown in **Table S5** and it reflects the strength of a linear relationship between a set of variables and the predicted output. The absolute value of this number indicates how related the variables and the output are, and the closer the number is to 1, the stronger the relationship. Having a Multiple R of 0.85 shows a strong linear relationship between the chosen parameters and the conversion to butyl butyrate [58]. This is further confirmed with an R^2 value of 0.723 and an adjusted R^2 of 0.659 showing that the majority of the obtained results in the three studies could be explained by the suggested

model. The average error of 5.19% and the comparison between the model-predicted results and the experimentally obtained values of the conversion to butyl butyrate shows that the model well represents the results obtained experimentally (**Table S6**). Additionally, having the significance F value lower than 0.05 means that the model is statistically acceptable in predicting the desired output [58].

Having the values of the parameters normalized, the regression coefficients estimated become valuable tools, not only for the prediction of the conversion to butyl butyrate given different parameters of UiO-66-based structures, but also in the engineering of these parameters. The regression weights help highlight the relative influence of each of the characteristics in boosting the catalytic activity of the structure. Moreover, comparing the a, b, and c weights of 6.87, 21.93, and 25.25 respectively for %A, %B, and %C, attributed to the level of incorporation of the different linkers, it could be clearly seen that the model assigned higher weight for the functionalized linker in the prediction of the conversion. This means that the addition of linkers with uncoordinated active functional groups had a better impact on the increase of the conversion than the addition of the terephthalic acid linkers as previously concluded. Additionally, the weight of the defects number was estimated to be 25.07, which is similar to that assigned for the incorporation of the linkers functionalized with two hydroxyl groups which reflect comparable importance of the defects number and the additional functional groups on the performance of the UiO-66 structures in this reaction. Moreover, the surface area and the catalyst loading were assigned 16.18 and 15.38 regression weights respectively, which also emphasizes a similar effect on the catalysis of the reaction which seems to be less significant when compared to the density of active sites as is previously discussed in our studies [39, 40]. The model also assigned an intercept value Cst of around 40% as the conversion to butyl butyrate if no catalyst is used in the reaction. This prediction is relatively accurate as around 45% conversion is obtained when no catalyst is used which is mainly due to the

autocatalytic effect of butyric acid itself as indicated in a previous study [39]. Besides the conclusions on the relative importance of these parameters in governing the conversion to butyl butyrate, the model predicts this conversion at an error of around 5% which makes it a valuable tool in predicting the conversion for design purposes while changing the MOFs parameters without having to actually synthesize the MOF or run the esterification reaction at all.

Conclusion

This study reports the use of MTV-UiO-66 structures as catalysts for butyl butyrate production. Besides the single component structures, two mixed-linker systems are synthesized: MTV-UiO-66$(COOH)_2$ which incorporates both terephthalic acid (A) and 1, 2, 4, 5-benzenetetracarboxylic acid (B), and MTV-UiO-66$(OH)_2$ which includes both terephthalic acid (A) and 2,5-Dihydroxyterephthalic acid (C), at three different ratios, yielding a total of nine structures. The obtained structures are fully characterized and showed homogeneous incorporation of the functionalized linkers within the MOF crystals, which also benefited from a high level of cluster defects thanks to the modulation synthesis conditions. The values of surface area and pore volume decreased with the increased level of functionalized linkers' incorporation, which is found to be slightly lower than the starting molar ratio as indicated by ^{1}H-NMR results. For both systems, MTV-UiO-66 incorporating starting molar percentages of 75% functionalized linkers and 25% BDC yielded the best performance with 89% and 92% of butyl butyrate conversion using UiO-66(1A:3B) and UiO-66(1A:3C) respectively, using only 1 wt% catalyst loading. This performance was attained using double the catalyst loading for highly defective single component functionalized structures in our previous studies, which highlights the success of using the multivariate approach to boost their catalytic activity. This is achieved by increasing the level of active sites density through partial functionalization while maintaining higher surface areas and pore volumes than the purely functionalized structures which allowed for easier access to these sites. However, not all MTV-MOFs perform better than their single linker counterparts which is caused by a sum of factors related to the density of active sites on one hand, and the internal diffusion limitations on the other. This further highlights the MOFs' characteristics that govern their catalytic activity which encouraged the development of a weighted linear regression model based on these characteristics. The calculation of the weights attributed to each of these characteristics is done in a way to find the

best fit to the experimental data of the 33 UiO-66 based catalysts developed throughout our studies on the production of butyl butyrate. The results showed that the density of active sites, through the number of defects or the functional groups on the linker, had a relatively higher impact than the levels of surface area and catalyst loading, where both of which had in turn comparable impact on the conversion prediction based on the model results. These interesting findings pave the way for the development of highly efficient UiO-66-based catalysts for biofuel production.

Associated Content

The supporting information file contain the following:

MOF catalysts synthesis procedure condition details, a narrow 2theta range of the PXRD patterns of the MTV-MOFs, ^{1}H-NMR spectra of all MTV-MOFs, parameters used to build the regression model, normalazied parameters used to build the regression model, the parameters suggested for the model along with their corresponding regression coefficients and p-values, the regression model statistics summary, and the model-predicted vs. experimentally obtained conversion to butyl butyrate and the average error between the two for the set of experiments done.

Acknowledgements

The authors gratefully acknowledge the funding provided by the American University of Beirut Research Board and the K. Shair Central Research Science Laboratory.

Conflict of interest

The authors declare no conflict of interest

References

1. Worldwatch, I. *Biofuels for Transport : Global Potential and Implications for Sustainable Energy and Agriculture*. 2012.
2. Awadallah, F. and E.H. Fini, *Transportation global environmental impact.* ITE journal., 2013. **83**(9).
3. Su, Y., et al., *Progress of microalgae biofuel's commercialization.* Renewable and Sustainable Energy Reviews, 2017. **74**(Supplement C): p. 402-411.
4. Jenkins, R.W., et al., *Potential renewable oxygenated biofuels for the aviation and road transport sectors.* Fuel Fuel, 2013. **103**(4): p. 593-599.
5. Sjöblom, M., et al., *In situ biocatalytic synthesis of butyl butyrate in diesel and engine evaluations.* ChemCatChem, 2017: p. 4529-4537.
6. Severini, F., et al., *Development of heterogeneous acid catalysts produced from the carbonization of Miscanthus x giganteus for the esterification of butyric acid to butyl butyrate with n-butanol.* JCTB Journal of Chemical Technology & Biotechnology, 2016. **91**(7): p. 2076-2084.
7. Zuoxiang, Z., et al., *Recent Developments on the Mechanism and Kinetics of Esterification Reaction Promoted by Various Catalysts*. 2012: INTECH Open Access Publisher.
8. Zeng, Z., et al., *Recent Developments on the Mechanism and Kinetics of Esterification Reaction Promoted by Various Catalysts.* 2012.
9. Lotero, E., et al., *Synthesis of Biodiesel via Acid Catalysis.* Ind. Eng. Chem. Res. Industrial & Engineering Chemistry Research, 2005. **44**(14): p. 5353-5363.
10. Li, C. and Y. Liu. *Bridging heterogeneous and homogeneous catalysis : concepts, strategies, and applications*. 2014.
11. Guldhe, A., et al., *Biodiesel synthesis from microalgal lipids using tungstated zirconia as a heterogeneous acid catalyst and its comparison with homogeneous acid and enzyme catalysts.* Fuel, 2017. **187**(Supplement C): p. 180-188.
12. Milina, M., S. Mitchell, and J. Pérez-Ramírez, *Prospectives for bio-oil upgrading via esterification over zeolite catalysts.* Catalysis Today, 2014. **235**(Supplement C): p. 176-183.
13. Avramidou, K.V., et al., *Esterification of free fatty acids using acidic metal oxides and supported polyoxometalate (POM) catalysts.* Molecular Catalysis, 2017. **439**(Supplement C): p. 60-71.
14. Kuzminska, M., R. Backov, and E.M. Gaigneaux, *Behavior of cation-exchange resins employed as heterogeneous catalysts for esterification of oleic acid with trimethylolpropane.* Applied Catalysis A: General, 2015. **504**(Supplement C): p. 11-16.
15. Hayes, D.J., *An examination of biorefining processes, catalysts and challenges.* CATTOD Catalysis Today, 2009. **145**(1): p. 138-151.
16. Yang, D. and B.C. Gates, *Catalysis by Metal Organic Frameworks: Perspective and Suggestions for Future Research.* ACS Catal. ACS Catalysis, 2019: p. 1779-1798.
17. Xu, C., et al., *Functional metal-organic frameworks for catalytic applications.* Coordination chemistry reviews, 2019. **388**: p. 268-292.
18. Nouar, F., et al., *Tuning the properties of the UiO-66 metal organic framework by Ce substitution.* Chemical communications (Cambridge, England), 2015. **51**(77): p. 14458-61.
19. Islamoglu, T., et al., *Postsynthetic Tuning of Metal-Organic Frameworks for Targeted Applications.* Accounts of chemical research, 2017. **50**(4): p. 805-813.

20. Hu, M.-L., et al., *Taking organic reactions over metal-organic frameworks as heterogeneous catalysis.* Microporous and mesoporous materials, 2018. **256**: p. 111-127.
21. James, S.L., *Metal-organic frameworks.* Chemical Society Reviews, 2003. **32**(5): p. 276-288.
22. Eddaoudi, M., et al., *Modular chemistry: secondary building units as a basis for the design of highly porous and robust metal-organic carboxylate frameworks.* Accounts of chemical research, 2001. **34**(4): p. 319-30.
23. Ren, J., et al., *Structural defects in metal-organic frameworks (MOFs): Formation, detection and control towards practices of interests.* CCR Coordination Chemistry Reviews, 2017. **349**: p. 169-197.
24. Kirlikovali, K.O., et al., *Zirconium-Based Metal–Organic Frameworks for the Catalytic Hydrolysis of Organophosphorus Nerve Agents.* ACS Applied Materials & Interfaces, 2020. **12**(13): p. 14702-14720.
25. Mortada, B., et al., *Postmetalated Zirconium Metal Organic Frameworks as a Highly Potent Bactericide.* Inorg. Chem. Inorganic Chemistry, 2017. **56**(8): p. 4739-4744.
26. Lin, R.-B., et al., *Exploration of porous metal-organic frameworks for gas separation and purification.* CCR Coordination Chemistry Reviews, 2019. **378**: p. 87-103.
27. Li, B., et al., *Porous Metal-Organic Frameworks for Gas Storage and Separation: What, How, and Why?* The journal of physical chemistry letters, 2014. **5**(20): p. 3468-79.
28. Lyu, J., et al., *Modular Synthesis of Highly Porous Zr-MOFs Assembled from Simple Building Blocks for Oxygen Storage.* ACS Applied Materials & Interfaces, 2019. **11**(45): p. 42179-42185.
29. Kumar, P., et al., *Metal-organic frameworks (MOFs) as futuristic options for wastewater treatment.* JIEC Journal of Industrial and Engineering Chemistry, 2018. **62**: p. 130-145.
30. Kreno, L.E., et al., *Metal-Organic Framework Materials as Chemical Sensors.* Chemical Reviews, 2012. **112**(2): p. 1105-1125.
31. Kang, Y.-S., et al., *Metal-organic frameworks with catalytic centers: From synthesis to catalytic application.* Coordination chemistry reviews, 2019. **378**: p. 262-280.
32. Cirujano, F.G., A. Corma, and F.X. Llabrés i Xamena, *Conversion of levulinic acid into chemicals: Synthesis of biomass derived levulinate esters over Zr-containing MOFs.* Chemical Engineering Science, 2015. **124**(Supplement C): p. 52-60.
33. Cirujano, F.G., A. Corma, and F.X. Llabrés i Xamena, *Zirconium-containing metal organic frameworks as solid acid catalysts for the esterification of free fatty acids: Synthesis of biodiesel and other compounds of interest.* Catalysis Today, 2015. **257**(Part 2): p. 213-220.
34. Panchenko, Timofeeva, and Jhung, *Acid-base properties and catalytic activity of metal-organic frameworks: A view from spectroscopic and semiempirical methods.* Catalysis Reviews, 2016. **58**(2): p. 209-307.
35. Trickett, C.A., et al., *Definitive molecular level characterization of defects in UiO-66 crystals.* Angewandte Chemie (International ed. in English), 2015. **54**(38): p. 11162-7.
36. Taddei, M., *When defects turn into virtues: The curious case of zirconium-based metal-organic frameworks.* CCR Coordination Chemistry Reviews, 2017. **343**: p. 1-24.
37. Canivet, J., M. Vandichel, and D. Farrusseng, *Origin of highly active metalorganic framework catalysts: defects? Defects!* DT Dalton Transactions, 2016. **45**(10): p. 4090-4099.

38. Wei, R., et al., *Tuning the properties of Zr6O8 nodes in the metal organic framework UiO-66 by selection of node-bound ligands and linkers.* Chem. Mater. Chemistry of Materials, 2019.
39. Jrad, A., et al., *Tuning acidity in zirconium-based metal organic frameworks catalysts for enhanced production of butyl butyrate.* APCATA Applied Catalysis A, General, 2019. **570**: p. 31-41.
40. Jrad, A., et al., *Structural engineering of Zr-based metal-organic framework catalysts for optimized biofuel additives production.* Chemical Engineering Journal, 2020. **382**: p. 122793.
41. Chen, S., et al., *Hydrogen storage properties of the novel crosslinked UiO-66-(OH)2.* HE International Journal of Hydrogen Energy, 2018. **43**(32): p. 15370-15377.
42. Yang, Q., et al., *A Water Stable Metal-Organic Framework with Optimal Features for CO2 Capture.* Angewandte Chemie International Edition, 2013. **52**(39): p. 10506–10510.
43. Deng, H., et al., *Multiple Functional Groups of Varying Ratios in Metal-Organic Frameworks.* Science, 2010. **327**(5967): p. 846-850.
44. Issa, R., et al., *Controlled growth and composition of multivariate metal-organic frameworks-199 via a reaction-diffusion process.* Nano Research, 2020.
45. Burrows, A.D., *Mixed-component metal–organic frameworks (MC-MOFs): enhancing functionality through solid solution formation and surface modifications.* CrystEngComm, 2011. **13**(11): p. 3623.
46. Burrows, A.D., et al., *Post-Synthetic Modification of Tagged Metal-Organic Frameworks.* Angewandte Chemie International Edition, 2008. **47**(44): p. 8482-8486.
47. Taddei, M., et al., *Mixed-linker UiO-66: structure-property relationships revealed by a combination of high-resolution powder X-ray diffraction and density functional theory calculations.* Physical chemistry chemical physics : PCCP, 2017. **19**(2): p. 1551-1559.
48. Kim, M., et al., *Postsynthetic modification at orthogonal reactive sites on mixed, bifunctional metal-organic frameworks.* Chemical communications (Cambridge, England), 2011. **47**(27): p. 7629-31.
49. Bunck, D.N. and W.R. Dichtel, *Mixed Linker Strategies for Organic Framework Functionalization.* Chemistry - A European Journal, 2013. **19**(3): p. 818-827.
50. Shearer, G.C., et al., *Defect Engineering: Tuning the Porosity and Composition of the Metal-Organic Framework UiO-66 via Modulated Synthesis.* Chemistry of Materials, 2016. **28**(11): p. 3749-3761.
51. Chaemchuen, S., et al., *Defect formation in metal-organic frameworks initiated by the crystal growth-rate and effect on catalytic performance.* YJCAT Journal of Catalysis, 2017. **354**: p. 84-91.
52. Shearer, G.C., et al., *Tuned to Perfection: Ironing Out the Defects in MetalOrganic Framework UiO-66.* Chem. Mater. Chemistry of Materials, 2014. **26**(14): p. 4068-4071.
53. Wu, H., et al., *Unusual and highly tunable missing-linker defects in zirconium metal-organic framework UiO-66 and their important effects on gas adsorption.* Journal of the American Chemical Society, 2013. **135**(28): p. 10525-32.
54. Zhou, et al., *Zirconium-containing UiO-66 as an efficient and reusable catalyst for transesterification of triglyceride with methanol.* JECHEM Journal of Energy Chemistry, 2016. **25**(5): p. 874-879.
55. Marx, S., et al., *Tuning functional sites and thermal stability of mixed-linker MOFs based on MIL-53(Al).* Dalton Transactions, 2010. **39**(16): p. 3795-3798.

56. Taddei, M., et al., *Mixed-linker UiO-66: structure–property relationships revealed by a combination of high-resolution powder X-ray diffraction and density functional theory calculations.* Physical Chemistry Chemical Physics, 2017. **19**(2): p. 1551-1559.
57. Dhakshinamoorthy, A., et al., *Intracrystalline diffusion in Metal Organic Framework during heterogeneous catalysis: Influence of particle size on the activity of MIL-100 (Fe) for oxidation reactions.* Dalton Trans. Dalton Transactions, 2011. **40**(40): p. 10719-10724.
58. Yan, X. and X.G. Su, *Linear Regression Analysis: Theory and Computing*. 2009: World Scientific Publishing Co., Inc.